Vapor−Liquid Equilibrium Data for the Nitrogen + *n*-Decane System from (344 to 563) K and at Pressures up to 50 MPa†

Fernando García-Sánchez,*,‡ Gaudencio Eliosa-Jiménez,§ Guadalupe Silva-Oliver,|| and Blanca E. García-Flores‡

Laboratorio de Termodinámica, Programa de Investigación en Ingeniería Molecular, Instituto Mexicano del Petróleo. Eje Central Lázaro Cárdenas 152, 07730 México, D.F., México, Facultad de Ingeniería Química, BUAP, 18 Sur y Av. San Claudio, Colonia San Manuel. C.P. 72570. Cd. Universitaria, Puebla, México, and Departamento de Ingeniería Química Petrolera, ESIQIE, Instituto Politécnico Nacional, Unidad Profesional Adolfo López Mateos, 07738 México, D.F., México

A static-analytical apparatus with visual sapphire windows and pneumatic capillary samplers has been used to obtain new vapor−liquid equilibrium data for the N_2 + $C_{10}H_{22}$ system over a wide temperature range from (344 to 563) K and at pressures up to 50 MPa. Equilibrium phase compositions and vapor−liquid equilibrium ratios are reported. The experimental data were modeled with the PR (Peng−Robinson) and PC-SAFT (perturbed-chain statistical association fluid theory) equations of state by using one-fluid mixing rules and a single temperature-independent interaction parameter. Results from the modeling effort showed that the PC-SAFT equation was superior to the PR equation in correlating the experimental data of the N_2 + $C_{10}H_{22}$ system over the whole temperature, pressure, and composition range studied.

Introduction

Knowledge of N_2 solubility in hydrocarbon compounds is very useful in relation to an optimal recovery strategy in enhanced oil recovery by gas N_2 injection. Solubilities of N_2 in paraffin, aromatic, and naphthenic compounds have already been studied (see ref 1 and references therein), but a lot of other mixtures remain to be investigated.

On the other hand, from the theoretical point of view, the phase behavior prediction of systems containing N_2 with hydrocarbons is a challenging task[2,3] due to that all binary N_2 + hydrocarbon fluid mixtures develop, except for methane, type III phase diagrams according to the classification scheme of van Konynenburg and Scott.[4] That is, type III mixtures exhibit two distinct critical curves, one starting at the critical point of the component with the higher critical temperature that goes to infinite pressures and the other critical curve starting at the critical point of the component with the lower critical temperature and meeting a three-phase line liquid−liquid−vapor at an upper critical end point. Therefore, it is important to carry out additional experimental phase equilibrium studies at elevated temperatures and pressures of N_2-containing binary systems along with some modeling effort using thermodynamic models to give the right qualitative and quantitative description of the phase behavior of N_2−hydrocarbon mixtures and thus providing a better understanding of phase behavior patterns that hydrocarbon mixtures develop during an enhanced oil recovery process by high-pressure N_2 injection. A wide discussion of the employment of N_2 in enhanced oil recovery is presented by de Leeuw[5] in his doctoral dissertation, whereas an application of miscible displacement with high-pressure N_2 injection for a naturally fractured thick carbonate reservoir containing light oil underlain by an aquifer has been recently reported by Mungan.[6]

To increase the experimental database of vapor−liquid equilibria for mixtures containing N_2 and a hydrocarbon, we have undertaken a systematic study of the phase behavior of N_2 + hydrocarbon mixtures at high pressures. Previously, we have reported vapor−liquid equilibrium data of N_2 + *n*-alkane mixtures over wide temperature ranges and pressures up to 50 MPa.[7−10] These studies are part of a research program where phase behavior is studied for enhanced oil recovery in selected Mexican fields by high-pressure N_2 injection.

In this work, we report new vapor−liquid equilibrium measurements for the system N_2 + $C_{10}H_{22}$ over the temperature range from (344 to 563) K and at pressures up to 50 MPa. Seven isotherms are reported in this study, which were determined in a high-pressure phase equilibrium apparatus of the static-analytical type using a sampling-analyzing process for determining the composition of the different coexisting phases.

The experimental data obtained in our measurements were correlated using the PR[11] and PC-SAFT[12] equations of state. The mixing rules used for these equations were the classical one-fluid mixing rules. For both models, a single temperature-independent interaction parameter was fitted to all experimental data.

Experimental Section

Materials. N_2 and He (carrier gas) were acquired from Aga Gas (Mexico) and Infra (Mexico), respectively, both with a certified purity greater than 99.999 mol %. *n*-Decane ($C_{10}H_{22}$) was purchased from Aldrich (USA) with a GLC minimum purity of 99 mol %. They were used without any further purification except for careful degassing of the $C_{10}H_{22}$.

Apparatus and Procedure. The apparatus and procedures employed in its operation have been previously described[7−10] and will not be repeated in detail in this report. Briefly, the apparatus consists mainly of an equilibrium cell, a sampling-analyzing system, a pressure transducer, two platinum temper-

* Author to whom correspondence should be addressed. Tel.: +52 55 9175 6574. E-mail: fgarcias@imp.mx.
† Part of the "Gerhard M. Schneider Festschrift".
‡ Instituto Mexicano del Petróleo.
§ BUAP.
|| Instituto Politécnico Nacional.

10.1021/je800881t CCC: $40.75 © 2009 American Chemical Society
Published on Web 03/03/2009

ature sensors, a magnetic stirring device, a timer and compressed-air control device for each sampler, an analytical system, and feeding and degassing circuits. This apparatus is based on the static-analytical method with fluid phase sampling and can be used to determine the multiphase equilibrium of binary and multicomponent systems between (313 and 673) K and pressures up to 60 MPa.

The equilibrium cell (made of titanium) has an internal volume of about 100 mL and holds two sapphire windows for visual observation. The cap of the cell, used for studies at high temperatures with up to three coexisting phases, holds the three sampling systems with capillaries of different lengths: the extremity of one capillary is at the top of the cell (vapor withdrawing), another one at the bottom of the cell (withdrawing of the dense liquid), and the third one in an intermediate position (light liquid phase withdrawing). The sampling-analyzing system is constituted of three Rolsi capillary samplers[13] connected altogether online with a gas chromatograph, which makes the apparatus very practical and accurate for measurements at high temperatures and pressures. The equilibrium cell can be maintained within ± 0.2 K for temperatures between (313 and 673) K by means of a high-temperature regulating air thermostat.

Temperature measurements in the equilibrium cell were monitored by using two Pt100 resistance thermometers, which are periodically calibrated against a 25 Ω reference platinum resistance thermometer (Tinsley Precision Instruments; UK). The resulting uncertainty of the two Pt100 probes is, usually, not higher than ± 0.02 K; however, drift in the temperature of the air oven makes the uncertainty of the temperature measurements ± 0.2 K. Pressure measurements were carried out by means of a pressure transducer (Sensonetics for temperatures up to 673 K), which is periodically calibrated against a dead-weight pressure balance. Pressure measurement uncertainties are estimated to be within ± 0.02 MPa for pressures up to 50 MPa.

The analytical work was carried out using a gas chromatograph (Varian 3800) equipped with a thermal conductivity detector (TCD), which is connected to a data acquisition system (Star GC Workstation, Ver. 5.3). The analytical column used is a Restek 3 % OV-101 column (mesh 100/120 Silcoport-W, silcosteel tube, length: 3 m, diameter: 3.175 mm). The TCD was used to detect the $C_{10}H_{22}$ and N_2 compounds. It was calibrated by injecting known amounts of $C_{10}H_{22}$ and N_2 through liquidtight (5 μL) and gastight (1000 μL) syringes, respectively. Calibration data were fitted to a quadratic polynomial, leading to an estimated mole fraction uncertainty less than 1 % for liquid and vapor phases on the whole concentration range.

Once the pressure transducer, platinum temperature probes, and chromatographic thermal conductivity detector have been calibrated, the system was preflushed with isopropyl alcohol and then dried under vacuum at 423 K. After drying under vacuum, the system was purged with N_2 to ensure that the last traces of solvents were removed. During an experimental run, the liquid component, previously degassed according to the method of Battino et al.,[14] is first introduced into the cell. The equilibrium cell and its loading lines are evacuated before filling it with the degassed liquid component. Once the desired temperature is reached and stabilized, the gaseous component, previously stored in a high-pressure cell, is carefully introduced into the equilibrium cell until the pressure of measurement. Then, the magnetic stirring device is activated to reach equilibrium, which is indicated by pressure stabilization. Pressure is adjusted by injecting again the gaseous component and activating the stirring device until reaching the desired pressure. After the equilibrium in the cell is achieved, measurements are performed using the capillary-sampling injectors, which are connected to the equilibrium cell by 0.1 mm internal diameter capillary tubes of different lengths. The samples are injected and vaporized directly into the carrier gas (He) stream of the gas chromatograph. For each equilibrium condition, at least 25 equilibrium samples are withdrawn using the pneumatic samplers and analyzed to check for measurement and repeatability. As the volume of the withdrawn samples is very small compared to the volume of the vapor or liquid present in the equilibrium cell, it is possible to withdraw many samples without disturbing the phase equilibrium. To avoid condensation and adsorption of the $C_{10}H_{22}$, the samplers and all of the lines for the gas stream are superheated to ensure that the whole of the samples is transferred to the chromatograph.

Table 1. Summary of Vapor−Liquid Equilibria for the N_2 + $C_{10}H_{22}$ System

ref	T/K	p/MPa	no. of points	remarks
15	310.9 to 410.9	1.72 to 34.47	89	$p-x-y$ data
16	344.3	4.02 to 34.64	6	$p-x$ data
17	344.3 to 410.9	3.91 to 16.04	21	$p-x$ data
18	323.2 to 348.2	2.88 to 4.23	7	$p-y$ data
19	323.2 to 398.2	4.23 to 10.09	9	$p-y$ data
20	263.2 to 310.9	0.20 to 20.10	44	$p-y$ data
this work	344.6 to 563.1	1.04 to 50.32	142	$p-x-y$ data

Results

The N_2 + $C_{10}H_{22}$ system has been previously studied by Azarnoosh and McKetta,[15] Llave and Chung,[16] Tong et al.,[17] Prausnitz and Benson,[18] D'Avila et al.,[19] and Pearce et al.[20] at different temperature and pressure conditions. Table 1 contains a summary of the earlier results, including those presented in this paper. The new measured phase equilibrium compositions for this binary system in terms of N_2 liquid and vapor mole fractions and their respective uncertainties, temperatures, and pressures are tabulated in Table 2. Average uncertainties in the phase compositions, due mainly to errors associated with sampling, are estimated to be ± 0.002 in the mole fraction on the whole concentration range. Error calculations were performed in the following way: from eq 1 relating mole fractions z_i (liquid or vapor) to chromatographic measurements

$$z_i = \frac{n_i}{\sum_{j=1}^{N} n_j} = \frac{n_i}{n_T} \qquad z_i = x_i \text{ or } y_i \tag{1}$$

we have the errors given by

$$\Delta z_i = \frac{1}{n_T^2}[(n_T - n_i)\Delta n_i + n_i \sum_{j \neq i}^{N} \Delta n_j] \tag{2}$$

where Δn_i and Δn_j are the mean quadratic deviations in mole number for components i and j, resulting from a data fitting on the results of the chromatographic detector calibration.

Table 2 also presents the vapor pressures of $C_{10}H_{22}$ at each temperature level. These values were calculated with the Wagner equation in the "3, 6" form using the parameters reported by Reid et al.[21] as follows

$$\ln(p_s/p_c) = (1 - \tau)^{-1}[-8.56523\tau + 1.97756\tau^{1.5} - 5.81971\tau^3 - 0.29982\tau^6] \qquad \tau = 1 - T/T_c \tag{3}$$

Table 2. Experimental Vapor−Liquid Equilibrium Data for the N_2 (1) + $C_{10}H_{22}$ (2) System at Different Temperatures[a]

p/MPa	x_1	$\pm \Delta x_1$	y_1	$\pm \Delta y_1$	K_1	K_2	p/MPa	x_1	$\pm \Delta x_1$	y_1	$\pm \Delta y_1$	K_1	K_2
						T/K = 344.6							
0.003[b]	0.0000		0.0000				24.49	0.2420	0.0030	0.9974	0.0032	4.1215	0.0034
1.46	0.0195	0.0060	0.9953	0.0034	51.0410	0.0048	27.01	0.2630	0.0025	0.9971	0.0030	3.7913	0.0039
2.12	0.0263	0.0012	0.9968	0.0020	37.9011	0.0033	29.61	0.2838	0.0020	0.9968	0.0029	3.5123	0.0045
2.99	0.0365	0.0045	0.9975	0.0022	27.3288	0.0026	32.06	0.2982	0.0042	0.9965	0.0026	3.3417	0.0050
4.99	0.0592	0.0044	0.9981	0.0011	16.8598	0.0020	34.61	0.3162	0.0022	0.9962	0.0025	3.1505	0.0056
6.99	0.0838	0.0045	0.9983	0.0019	11.9129	0.0019	37.09	0.3341	0.0016	0.9959	0.0018	2.9808	0.0062
9.40	0.1097	0.0059	0.9984	0.0018	9.1012	0.0018	39.58	0.3467	0.0026	0.9955	0.0017	2.8714	0.0069
12.03	0.1343	0.0018	0.9983	0.0019	7.4334	0.0020	42.03	0.3617	0.0019	0.9950	0.0014	2.7509	0.0078
14.44	0.1580	0.0017	0.9982	0.0020	6.3177	0.0021	44.43	0.3777	0.0014	0.9945	0.0013	2.6330	0.0088
17.00	0.1812	0.0013	0.9980	0.0020	5.5077	0.0024	47.01	0.3902	0.0017	0.9941	0.0014	2.5477	0.0097
19.63	0.2025	0.0043	0.9978	0.0023	4.9274	0.0028	48.78	0.3985	0.0017	0.9936	0.0014	2.4934	0.0106
22.23	0.2264	0.0025	0.9976	0.0027	4.4064	0.0031	49.91	0.4036	0.0024	0.9932	0.0013	2.4609	0.0114
						T/K = 377.4							
0.01[b]	0.0000		0.0000				26.96	0.2891	0.0027	0.9945	0.0021	3.4400	0.0077
2.23	0.0307	0.0035	0.9932	0.0026	32.3518	0.0070	29.54	0.3106	0.0035	0.9940	0.0019	3.2003	0.0087
4.55	0.0601	0.0031	0.9958	0.0015	16.5691	0.0045	32.04	0.3322	0.0024	0.9935	0.0018	2.9907	0.0097
5.01	0.0659	0.0036	0.9960	0.0017	15.1138	0.0043	34.44	0.3483	0.0029	0.9932	0.0016	2.8516	0.0104
6.97	0.0902	0.0027	0.9963	0.0014	11.0455	0.0041	37.02	0.3679	0.0027	0.9927	0.0015	2.6983	0.0115
9.48	0.1195	0.0023	0.9965	0.0016	8.3389	0.0040	39.50	0.3863	0.0022	0.9920	0.0014	2.5680	0.0130
11.98	0.1480	0.0031	0.9964	0.0020	6.7324	0.0042	42.02	0.4061	0.0020	0.9913	0.0014	2.4410	0.0146
14.46	0.1748	0.0025	0.9963	0.0018	5.6997	0.0045	44.01	0.4205	0.0016	0.9907	0.0014	2.3560	0.0160
16.98	0.2009	0.0026	0.9961	0.0020	4.9582	0.0049	46.89	0.4417	0.0017	0.9896	0.0013	2.2404	0.0186
19.44	0.2235	0.0030	0.9958	0.0014	4.4555	0.0054	48.27	0.4480	0.0019	0.9887	0.0012	2.2069	0.0205
21.99	0.2474	0.0027	0.9955	0.0017	4.0238	0.0060	49.56	0.4580	0.0015	0.9882	0.0012	2.1576	0.0218
24.46	0.2682	0.0024	0.9950	0.0024	3.7099	0.0068							
						T/K = 410.9							
0.04[b]	0.0000		0.0000				24.68	0.3078	0.0022	0.9893	0.0018	3.2141	0.0155
1.94	0.0352	0.0023	0.9823	0.0018	27.9063	0.0183	26.87	0.3295	0.0021	0.9887	0.0017	3.0006	0.0169
3.21	0.0564	0.0032	0.9877	0.0015	17.5124	0.0130	29.46	0.3546	0.0021	0.9877	0.0014	2.7854	0.0191
4.62	0.0759	0.0026	0.9899	0.0015	13.0422	0.0109	32.13	0.3786	0.0017	0.9870	0.0014	2.6070	0.0209
5.48	0.0876	0.0023	0.9906	0.0018	11.3082	0.0103	34.47	0.3974	0.0018	0.9864	0.0016	2.4821	0.0226
7.39	0.1145	0.0019	0.9915	0.0015	8.6594	0.0096	37.01	0.4189	0.0017	0.9852	0.0020	2.3519	0.0255
9.62	0.1428	0.0025	0.9917	0.0016	6.9447	0.0097	39.35	0.4391	0.0015	0.9840	0.0020	2.2409	0.0285
12.07	0.1729	0.0032	0.9916	0.0015	5.7351	0.0102	42.01	0.4611	0.0015	0.9819	0.0024	2.1295	0.0336
14.37	0.2003	0.0024	0.9915	0.0016	4.9501	0.0106	44.41	0.4815	0.0014	0.9808	0.0023	2.0370	0.0370
17.07	0.2317	0.0023	0.9912	0.0013	4.2779	0.0115	47.04	0.5046	0.0013	0.9796	0.0021	1.9413	0.0412
19.58	0.2563	0.0026	0.9905	0.0015	3.8646	0.0128	49.50	0.5234	0.0012	0.9778	0.0021	1.8682	0.0466
21.99	0.2808	0.0022	0.9900	0.0021	3.5256	0.0139	50.32	0.5300	0.0013	0.9771	0.0019	1.8436	0.0487
						T/K = 463.7							
0.15[b]	0.0000		0.0000				21.91	0.3315	0.0021	0.9705	0.0013	2.9276	0.0441
1.83	0.0384	0.0013	0.9299	0.0024	24.2161	0.0729	24.46	0.3656	0.0017	0.9688	0.0018	2.6499	0.0492
2.25	0.0461	0.0028	0.9385	0.0020	20.3579	0.0645	27.06	0.3939	0.0021	0.9673	0.0016	2.4557	0.0540
3.19	0.0634	0.0025	0.9513	0.0014	15.0047	0.0520	29.43	0.4254	0.0017	0.9653	0.0016	2.2692	0.0604
4.51	0.0855	0.0023	0.9604	0.0013	11.2327	0.0433	31.96	0.4544	0.0017	0.9629	0.0013	2.1191	0.0680
5.31	0.0993	0.0027	0.9632	0.0015	9.6999	0.0409	34.58	0.4851	0.0016	0.9611	0.0013	1.9812	0.0755
6.99	0.1263	0.0025	0.9673	0.0016	7.6587	0.0374	36.98	0.5149	0.0013	0.9578	0.0013	1.8602	0.0870
9.46	0.1643	0.0023	0.9709	0.0013	5.9093	0.0348	39.54	0.5433	0.0013	0.9532	0.0013	1.7545	0.1025
12.07	0.2001	0.0021	0.9725	0.0014	4.8601	0.0344	42.10	0.5728	0.0011	0.9502	0.0013	1.6589	0.1166
14.48	0.2351	0.0026	0.9726	0.0013	4.1370	0.0358	44.46	0.5999	0.0011	0.9464	0.0014	1.5776	0.1340
17.01	0.2698	0.0023	0.9718	0.0013	3.6019	0.0386	47.27	0.6285	0.0011	0.9381	0.0019	1.4926	0.1666
19.55	0.3023	0.0023	0.9718	0.0012	3.2147	0.0404	49.84	0.6553	0.0009	0.9313	0.0015	1.4212	0.1993
						T/K = 503.0							
0.35[b]	0.0000		0.0000				16.94	0.3033	0.0024	0.9388	0.0021	3.0953	0.0878
1.52	0.0279	0.0037	0.7515	0.0059	26.9355	0.2556	19.12	0.3370	0.0021	0.9387	0.0019	2.7855	0.0925
2.14	0.0406	0.0028	0.8122	0.0039	20.0049	0.1957	21.93	0.3802	0.0022	0.9368	0.0018	2.4640	0.1020
2.75	0.0535	0.0028	0.8477	0.0033	15.8449	0.1609	24.38	0.4186	0.0021	0.9339	0.0016	2.2310	0.1137
3.64	0.0705	0.0023	0.8779	0.0027	12.4525	0.1314	26.74	0.4561	0.0017	0.9309	0.0015	2.0410	0.1270
4.53	0.0878	0.0022	0.8957	0.0026	10.2016	0.1143	29.60	0.5012	0.0016	0.9239	0.0017	1.8434	0.1526
5.61	0.1072	0.0026	0.9084	0.0027	8.4739	0.1026	32.05	0.5409	0.0014	0.9161	0.0019	1.6937	0.1827
6.98	0.1317	0.0026	0.9179	0.0035	6.9696	0.0946	34.88	0.5878	0.0013	0.9001	0.0044	1.5313	0.2424
9.49	0.1758	0.0027	0.9289	0.0032	5.2838	0.0863	37.25	0.6317	0.0012	0.8849	0.0043	1.4008	0.3125
11.95	0.2192	0.0023	0.9358	0.0024	4.2692	0.0822	40.22	0.7053	0.0011	0.8487	0.0045	1.2033	0.5134
14.42	0.2613	0.0021	0.9388	0.0020	3.5928	0.0828							
						T/K = 533.5							
0.61[b]	0.0000		0.0000				9.37	0.1955	0.0024	0.8752	0.0023	4.4767	0.1551
1.04	0.0152	0.0023	0.4458	0.0072	29.3289	0.5628	11.95	0.2464	0.0030	0.8872	0.0018	3.6006	0.1497
1.49	0.0260	0.0024	0.5759	0.0063	22.1500	0.4354	14.48	0.2984	0.0024	0.8899	0.0018	2.9822	0.1569
2.10	0.0402	0.0028	0.6677	0.0056	16.6095	0.3462	16.96	0.3452	0.0026	0.8905	0.0015	2.5797	0.1672
2.68	0.0525	0.0024	0.7204	0.0058	13.7219	0.2951	19.51	0.3949	0.0024	0.8854	0.0018	2.2421	0.1894
3.65	0.0735	0.0023	0.7755	0.0056	10.5510	0.2423	22.08	0.4455	0.0022	0.8766	0.0023	1.9677	0.2225
4.55	0.0938	0.0025	0.8069	0.0054	8.6023	0.2131	24.48	0.4988	0.0020	0.8655	0.0023	1.7352	0.2684
5.55	0.1167	0.0024	0.8322	0.0042	7.1311	0.1900	27.03	0.5610	0.0018	0.8445	0.0024	1.5053	0.3542
6.95	0.1452	0.0025	0.8538	0.0032	5.8802	0.1710	29.66	0.6239	0.0009	0.7848	0.0047	1.2579	0.5722
						T/K = 563.1							
0.97[b]	0.0000		0.0000				9.50	0.2265	0.0024	0.7808	0.0010	3.4472	0.2834
1.53	0.0212	0.0020	0.3473	0.0029	16.3821	0.6668	11.94	0.2891	0.0023	0.7975	0.0016	2.7586	0.2849
2.14	0.0371	0.0024	0.4794	0.0021	12.9218	0.5407	14.49	0.3566	0.0025	0.7964	0.0012	2.2333	0.3164
2.66	0.0526	0.0025	0.5604	0.0017	10.6540	0.4640	15.72	0.3945	0.0018	0.7900	0.0012	2.0025	0.3468
3.50	0.0735	0.0026	0.6402	0.0013	8.7102	0.3883	17.00	0.4305	0.0024	0.7766	0.0012	1.8039	0.3923
4.54	0.0997	0.0022	0.6895	0.0010	6.9157	0.3449	19.05	0.5000	0.0035	0.7375	0.0012	1.4750	0.5250
5.62	0.1275	0.0029	0.7179	0.0010	5.6306	0.3233	19.64	0.5373	0.0043	0.7120	0.0012	1.3251	0.6224
7.01	0.1632	0.0027	0.7488	0.0010	4.5882	0.3002							

[a] $\Delta T = \pm 0.2$ K; $\Delta p = \pm 0.02$ MPa. [b] Calculated vapor pressure of pure $C_{10}H_{22}$.

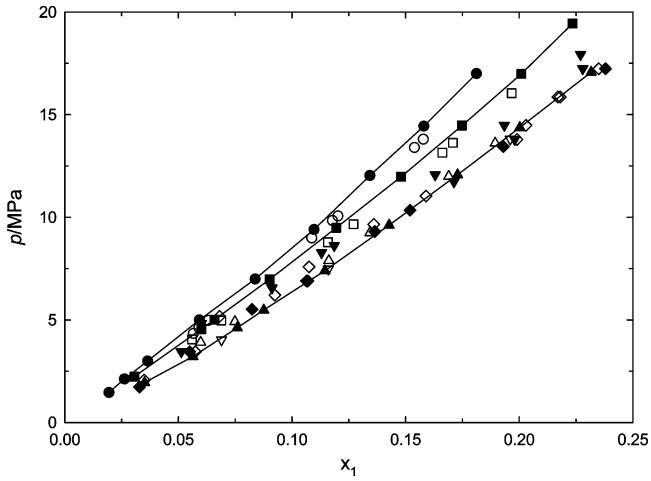

Figure 1. Experimental solubilities of N_2 (1) in $C_{10}H_{22}$ (2). This work: ●, 344.6 K; ■, 377.4 K; ▲, 410.9 K. Ref 15: ▼, 344.3 K; ◇, 377.6 K; ◆, 410.9 K. Ref 16: ▽, 344.3 K. Ref 17: ○, 344.3 K; □, 377.6 K; △, 410.9 K. Solid lines used to better identify the experimental data of this work.

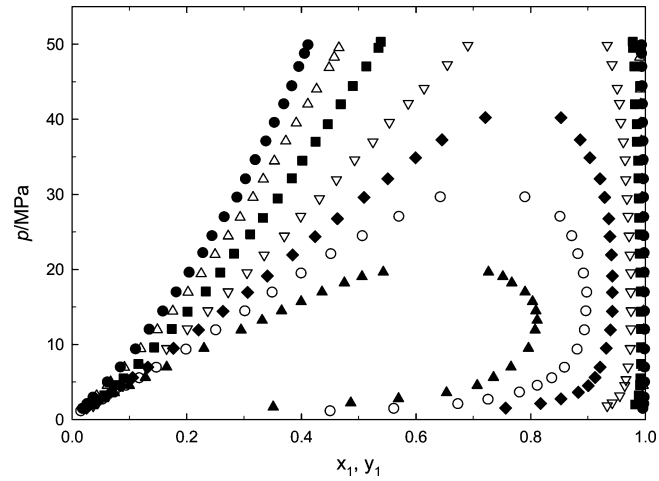

Figure 2. Experimental pressure−composition phase diagram for the N_2 (1) + $C_{10}H_{22}$ (2) system: ●, 344.6 K; △, 377.4 K; ■, 410.9 K; ▽, 463.7 K, ◆, 503.0 K; ○, 533.5 K; ▲, 563.1 K.

where p_s is the vapor pressure in MPa; p_c is the critical pressure in MPa; T is the temperature in K; and T_c is the critical temperature in K.

The calculated K values, defined as the equilibrium ratio between the vapor and liquid for each component at a given temperature and pressure, are also given in Table 2. This table shows that, for all the isotherms studied, N_2 has K values higher than 1 whereas $C_{10}H_{22}$ has K values lower than unity, which indicates that the N_2 concentrates in the vapor phase whereas $C_{10}H_{22}$ does it in the liquid phase.

Figure 1 shows the experimental solubilities of N_2 in the $C_{10}H_{22}$-rich liquid phase on a pressure−composition diagram at (344.6, 377.4, and 410.9) K along with the solubility results of Azarnoosh and McKetta,[15] Llave and Chung,[16] and Tong et al.[17] reported at about the same temperatures. In general, this figure shows that our experimental results are in good agreement with those determined by Tong et al.,[17] but they differ from those reported by the other authors. Similar conclusions were obtained by Tong et al.[17] who made comparisons of their N_2 + $C_{10}H_{22}$ data with those of Azarnoosh and McKetta[15] and Llave and Chung[16] in terms of the deviation in the solubility (liquid mole fraction of N_2) predicted by the PR[11] equation of state from the measured value. After a sensitive analysis of difference in data sets (not the magnitude of the deviation of either data set from the PR equation), these authors found quite a disagreement between their data and those of Azarnoosh and McKetta[15] and Llave and Chung.[16]

Figure 2 shows the results of the vapor−liquid equilibrium data obtained on a pressure−composition diagram for the seven experimental temperatures studied. In this figure, it can be observed that the solubility of N_2 in the $C_{10}H_{22}$-rich liquid phase increases as pressure increases for all isotherms investigated and that the solubility of N_2 in the $C_{10}H_{22}$-rich liquid phase decreases with decreasing temperature; i.e., a trend of increasing solubility of N_2 in the $C_{10}H_{22}$-rich liquid phase is observed as temperature and pressure increase.

Isotherms obtained above the critical temperature of N_2 (T_c = 126.2 K) end up in the mixture critical point, which was approached by adding carefully small quantities of N_2 to avoid upsetting the phase equilibrium. After every step of adding N_2, the cell content was stirred about four hours before withdrawing the samples of the equilibrium phases. It is worth mentioning that the measurements at (503.0, 533.5, and 563.1) K and (40.22, 29.66, and 19.64) MPa, respectively, were associated to an opalescence phenomenon, indicating the proximity of a critical state for this mixture; however, it was not possible to attain this terminal state due to that the apparatus is not suitable to measure this point directly. When the pressure was increased just above the critical point, only one phase was observed.

Table 3. Estimated Mixture Critical Data for the N_2 (1) + $C_{10}H_{22}$ (2) System

T/K	p/MPa	x_1	T/K	p/MPa	x_1
337.7[a]	220.0[a]	-	460.2[a]	60.0[a]	-
342.7[a]	200.0[a]	-	463.7	57.21	0.8714
349.2[a]	180.0[a]	-	486.7[a]	50.0[a]	-
357.2[a]	160.0[a]	-	503.0	41.72	0.7879
367.7[a]	140.0[a]	-	517.2[a]	40.0[a]	-
381.7[a]	120.0[a]	-	533.5	30.45	0.7013
400.7[a]	100.0[a]	-	563.1	20.34	0.6202
425.7[a]	80.0[a]	-	617.7[b]	2.104[b]	0.0000

[a] Data from Wirths.[22] [b] Critical point of pure $C_{10}H_{22}$.[27]

All isotherms studied in this work lie between the critical temperatures for the two components of this system. Since the equilibrium ratios for the two components converge to unity at the critical point of the mixture, then it is possible to obtain the critical pressure corresponding to each experimental temperature from the K values versus pressure diagram. Here, we estimated the mixture critical point for each isotherm by adjusting a series of pressure−composition data to Legendre polynomials. Once having correlated these data, the pressure−composition phase diagram is calculated to locate the maximum pressure. For a system with two components, this maximum corresponds to the critical pressure of the mixture at constant temperature. The composition associated to this maximum pressure corresponds to the critical composition of the mixture. The estimated numerical values of the critical points for the N_2 + $C_{10}H_{22}$ system are reported in Table 3, including the $p(T)$ critical data reported by Wirths[22] in his doctoral dissertation.

Figure 3 shows the isotherms plotted in a log K value versus log pressure diagram. In this figure, there are two branches for each isotherm, one for each component, which will converge at the mixture critical point, where the K values are equal to the unity. The degree of smoothness of the curve for each isotherm reflects the internal consistency of the data; however, it would be convenient to subject these data to a thermodynamic consistency test involving comparison between experimental and calculated vapor phase mole fractions by using, for instance,

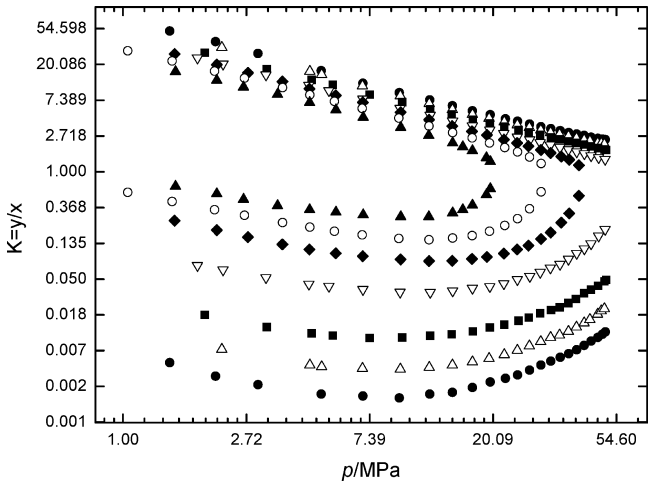

Figure 3. Effect of pressure on vapor−liquid equilibrium ratios for the N_2 (1) + $C_{10}H_{22}$ (2) system: ●, 344.6 K; △, 377.4 K; ■, 410.9 K; ▽, 463.7 K; ◆, 503.0 K; ○, 533.5 K; ▲, 563.1 K. N_2: *K* values higher than 1. $C_{10}H_{22}$: *K* values lower than 1.

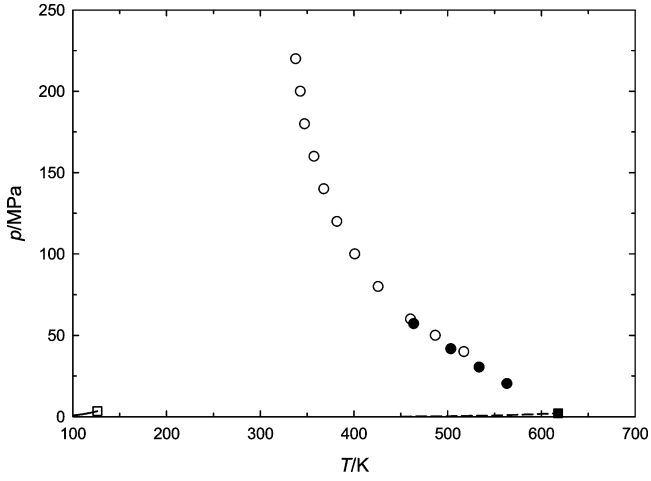

Figure 4. Pressure−temperature phase diagram for the N_2 + $C_{10}H_{22}$ system. This work: ●, mixture critical points. Ref 22: ○, mixture critical points. Ref 27: □, critical point of N_2; ■, critical point of $C_{10}H_{22}$. Solid line: vapor pressure of N_2. Dashed line: vapor pressure of $C_{10}H_{22}$.

the procedure given by Christiansen and Fredenslund[23] or the one given by Won and Prausnitz.[24]

The mixture critical data reported in Table 3 were plotted in a pressure−temperature diagram shown in Figure 4. In this figure, the vapor−liquid coexistence region studied in this work is bounded by three lines: the vapor pressure curve of pure N_2, the vapor pressure curve of pure $C_{10}H_{22}$, and the mixture critical line (N_2 + $C_{10}H_{22}$). An inspection of this figure shows that, starting at the critical point of pure $C_{10}H_{22}$, the mixture critical line runs to lower temperatures and higher pressures exhibiting a positive curvature. The data displayed in Figure 4 allow suggesting that the system N_2 + $C_{10}H_{22}$ is a type III system according to the classification of van Konynenburg and Scott.[4] Notwithstanding, to substantiate this claim, it is necessary to know about the other critical line that departs from the critical point of pure N_2 and whether this system exhibits a three-phase line liquid−liquid−vapor. Unfortunately, we have no experimental evidence of these phase equilibrium phenomena for this system because they occur at low temperatures and the apparatus used in this work is limited to be used at moderate and high temperatures. Moreover, due to that the melting point of $C_{10}H_{22}$ (243.5 K) is much higher than the critical temperature of N_2 (126.2 K), it is likely that a solid phase may appear in the system at the temperature around 126 K so that no simple liquid−liquid−vapor equilibrium can be observed.

Modeling

It is well-known that mixtures containing components that markedly differ in their critical temperatures (e.g., N_2 + hydrocarbon mixtures) behave highly asymmetrically so that the calculation of phase equilibria using an equation of state with pure-component information only is generally unsatisfactory. Thus, to increase the usefulness of the combining rules in the equations of state for predicting the phase behavior of the N_2 + $C_{10}H_{22}$ system, we have estimated the interaction parameter for the PR[11] and PC-SAFT[12] equations of state by fitting the experimental vapor−liquid equilibrium data presented in Table 2 for this system. These equations of state were selected in this work due to their wide use for the calculation of vapor−liquid equilibria for fluid mixtures, including those mixtures encountered in the natural-gas and petroleum industries.

The explicit form of the PR equation of state[11] can be written as

$$p = \frac{RT}{v - b} - \frac{a(T)}{v(v + b) + b(v - b)} \tag{4}$$

where constants a and b for pure components are related to

$$a = 0.45724\frac{RT_c}{p_c}\alpha(T_r) \tag{5}$$

$$b = 0.07780\frac{RT_c}{p_c} \tag{6}$$

and $\alpha(T_r)$ is expressed in terms of the acentric factor ω as

$$\alpha(T_r) = [1 + (0.37464 + 1.5422\omega - 0.26992\omega^2)(1 - T_r^{1/2})]^2 \tag{7}$$

For mixtures, constants a and b are given by

$$a = \sum_{i=1}^{N}\sum_{j=1}^{N} x_i x_j a_{ij} \tag{8}$$

$$b = \sum_{i=1}^{N} x_i b_i \tag{9}$$

and a_{ij} is defined as

$$a_{ij} = (1 - k_{ij})\sqrt{a_i a_j} \qquad k_{ij} = k_{ji};\ k_{ii} = 0 \tag{10}$$

where k_{ij} is an interaction parameter characterizing the binary mixture formed by components i and j. Equation 4 can be written in terms of the compressibility factor Z, as

$$Z^3 - (1 - B)Z^2 + (A - 3B^2 - 2B)Z - (AB - B^2 - B^3) = 0 \tag{11}$$

where $A = ap/(RT)^2$ and $B = bp/(RT)$.

The expression for the fugacity coefficient of component i is given by

$$\ln \varphi_i = \frac{b_i}{b}(Z-1) - \ln(Z-B) - \frac{A}{2\sqrt{2}B}\left(\frac{2\sum_{j=1}^{N} x_j a_{ij}}{a} - \frac{b_i}{b}\right)\ln\left(\frac{Z+(1+\sqrt{2})B}{Z+(1-\sqrt{2})B}\right) \quad (12)$$

In the PC-SAFT equation of state,[12] the molecules are conceived to be chains composed of spherical segments in which the pair potential for the segment of a chain is given by a modified square-well potential.[25] Nonassociating molecules are characterized by three pure-component parameters: the temperature-independent segment diameter σ, the depth of the potential ε, and the number of segments per chain m.

The PC-SAFT equation of state written in terms of the Helmholtz energy for an N-component mixture of nonassociating chains consists of a hard-chain reference contribution and a perturbation contribution to account for the attractive interactions. In terms of reduced quantities, this equation can be expressed as

$$\tilde{a}^{\mathrm{res}} = \tilde{a}^{\mathrm{hc}} + \tilde{a}^{\mathrm{disp}} \quad (13)$$

The hard-chain reference contribution is given by

$$\tilde{a}^{\mathrm{hc}} = \bar{m}\tilde{a}^{\mathrm{hs}} - \sum_{i=1}^{N} x_i(m_i - 1)\ln g_{ii}^{\mathrm{hs}}(\sigma_{ii}) \quad (14)$$

where $\bar{m}$ is the mean segment number in the mixture

$$\bar{m} = \sum_{i=1}^{N} x_i m_i \quad (15)$$

The Helmholtz energy of the hard-sphere fluid is given on a per-segment basis as

$$\tilde{a}^{\mathrm{hs}} = \frac{1}{\zeta_0}\left[\frac{3\zeta_1\zeta_2}{(1-\zeta_3)} + \frac{\zeta_2^3}{\zeta_3(1-\zeta_3)^2} + \left(\frac{\zeta_2^3}{\zeta_3^2} - \zeta_0\right)\ln(1-\zeta_3)\right] \quad (16)$$

and the radial distribution function of the hard-sphere fluid is

$$g_{ij}^{\mathrm{hs}} = \frac{1}{(1-\zeta_3)} + \left(\frac{d_i d_j}{d_i + d_j}\right)\frac{3\zeta_2}{(1-\zeta_3)^2} + \left(\frac{d_i d_j}{d_i + d_j}\right)^2 \frac{2\zeta_2^2}{(1-\zeta_3)^3} \quad (17)$$

with ζ_k defined as

$$\zeta_k = \frac{\pi}{6}\rho\sum_{i=1}^{N} x_i m_i d_i^k \qquad k = 0, 1, 2, 3 \quad (18)$$

The temperature-dependent segment diameter d_i of component i is given by

$$d_i = \sigma_i\left[1 - 0.12\exp\left(-3\frac{\varepsilon_i}{kT}\right)\right] \quad (19)$$

where k is the Boltzmann constant and T is the absolute temperature.

The dispersion contribution to the Helmholtz energy is given by

$$\tilde{a}^{\mathrm{disp}} = -2\pi\rho I_1(\eta, \bar{m})\overline{m^2\varepsilon\sigma^3} - \pi\rho\bar{m}\left(1 + Z^{\mathrm{hc}} + \rho\frac{\partial Z^{\mathrm{hc}}}{\partial\rho}\right)^{-1} I_2(\eta, \bar{m})\overline{m^2\varepsilon^2\sigma^3} \quad (20)$$

where Z^{hc} is the compressibility factor of the hard-chain reference contribution, and

$$\overline{m^2\varepsilon\sigma^3} = \sum_{i=1}^{N}\sum_{j=1}^{N} x_i x_j m_i m_j\left(\frac{\varepsilon_{ij}}{kT}\right)\sigma_{ij}^3 \quad (21)$$

$$\overline{m^2\varepsilon^2\sigma^3} = \sum_{i=1}^{N}\sum_{j=1}^{N} x_i x_j m_i m_j\left(\frac{\varepsilon_{ij}}{kT}\right)^2\sigma_{ij}^3 \quad (22)$$

The parameters for a pair of unlike segments are obtained by using conventional combining rules

$$\sigma_{ij} = \frac{1}{2}(\sigma_i + \sigma_j) \quad (23)$$

$$\varepsilon_{ij} = \sqrt{\varepsilon_i\varepsilon_j}(1 - k_{ij}) \quad (24)$$

where k_{ij} is a binary interaction parameter, which is introduced to correct the segment−segment interactions of unlike chains.

The terms $I_1(\eta, \bar{m})$ and $I_2(\eta, \bar{m})$ in eq 20 are calculated by simple power series in density

$$I_1(\eta, \bar{m}) = \sum_{i=0}^{6} a_i(\bar{m})\eta^i \quad (25)$$

$$I_2(\eta, \bar{m}) = \sum_{i=0}^{6} b_i(\bar{m})\eta^i \quad (26)$$

where the coefficients a_i and b_i depend on the chain length as given in Gross and Sadowski.[12]

The density to a given system pressure p^{sys} is determined iteratively by adjusting the reduced density η until $p^{\mathrm{calc}} = p^{\mathrm{sys}}$. For a converged value of η, the number density of molecules ρ, given in Å^{-3}, is calculated from

$$\rho = \frac{6}{\pi}\eta\left(\sum_{i=1}^{N} x_i m_i d_i^3\right)^{-1} \quad (27)$$

Using Avogadro's number and appropriate conversion factors, ρ produces the molar density in different units such as kmol·mol^{-3}.

Equations for the compressibility factor are derived from the relation

$$Z = 1 + \eta\left(\frac{\partial \tilde{a}^{res}}{\partial \eta}\right)_{T,x_i} = 1 + Z^{hc} + Z^{disp} \qquad (28)$$

The pressure p can be calculated in units of Pa = N·m^{-2} by applying the relation

$$p = ZkT\rho\left(10^{10}\frac{\text{Å}}{m}\right)^3 \qquad (29)$$

The expression for the fugacity coefficient of component i is given by

$$\ln \varphi_i = \left[\frac{\partial(n\tilde{a}^{res})}{\partial n_i}\right]_{\rho,T,n_{j\neq i}} + (Z - 1) - \ln Z \qquad (30)$$

where

$$\left[\frac{\partial(n\tilde{a}^{res})}{\partial n_i}\right]_{\rho,T,n_{j\neq i}} = \tilde{a}^{res} + \left(\frac{\partial \tilde{a}^{res}}{\partial x_i}\right)_{\rho,T,x_{j\neq i}} - \sum_{k=1}^{N}\left[x_k\left(\frac{\partial \tilde{a}^{res}}{\partial x_k}\right)_{\rho,T,x_{j\neq k}}\right] \qquad (31)$$

In eq 31, partial derivatives with respect to mole fractions are calculated regardless of the summation restriction $\sum_{i=1}^{N} x_i = 1$.

The binary interaction parameter k_{ij}, defined in eqs 10 and 24 for the PR and PC-SAFT equations of state, respectively, was estimated by minimizing the sum of squared relative deviations of bubble-point pressures and the sum of squared deviations in mole fraction of phase equilibrium compositions. The calculation of the phase equilibria was carried out by minimization of the Gibbs energy using stability tests (based on the tangent plane criterion) to find the most stable state of the system, according to the solution approach presented by Justo-García et al.[26] Physical properties of N_2 and $C_{10}H_{22}$ (i.e., critical temperature T_c, critical pressure p_c, and acentric factor ω) for the PR equation of state were taken from Ambrose,[27] while the three pure-component parameters (i.e., temperature-independent segment diameter σ, depth of the potential ε, and number of segments per chain m) of these compounds for the PC-SAFT equation of state were taken from Gross and Sadowski.[12]

The simplex optimization procedure of Nelder and Mead[28] with convergence accelerated by the Wegstein algorithm[29] was used in the computations by searching the minimum of the following objective functions

$$S_1 = \sum_{i=1}^{M}\left[\left(\frac{p_i^{exp} - p_i^{calc}}{p_i^{exp}}\right)^2 + (y_i^{exp} - y_i^{calc})^2\right] \qquad (32)$$

for the bubble-point pressure method and

$$S_2 = \sum_{i=1}^{M}[(x_i^{exp} - x_i^{calc})^2 + (y_i^{exp} - y_i^{calc})^2] \qquad (33)$$

for the flash calculation method.

Table 4. Estimated Binary Interaction Parameters for the N_2 (1) + $C_{10}H_{22}$ (2) System

PR equation of state				PC-SAFT equation of state			
k_{12}	σ_P	σ_x	σ_y	k_{12}	σ_P	σ_x	σ_y
Bubble-Point Pressure Method							
0.1597	10.0		2.6	0.1329	7.2		1.3
Flash Method							
0.1433		2.4	2.6	0.1344		1.9	1.7

In these equations, $p_i^{exp} - p_i^{calc}$, $x_i^{exp} - x_i^{calc}$, and $y_i^{exp} - y_i^{calc}$ are the residuals between the experimental and calculated values of, respectively, bubble-point pressures, liquid mole fractions, and vapor mole fractions for an experiment i, and M is the total number of experiments.

Once minimization of objective functions S_1 and S_2 was performed, the agreement between calculated and experimental values was established through the standard percent relative deviation in pressure, σ_P, and standard percent deviation in mole fraction for the liquid, σ_x, and vapor, σ_y, phases of the lightest component

$$\sigma_P = 100\left[\frac{1}{M}\sum_{i=1}^{M}\left(\frac{p_i^{exp} - p_i^{calc}}{p_i^{exp}}\right)^2\right]^{1/2} \qquad (34)$$

$$\sigma_x = 100\left[\frac{1}{M}\sum_{i=1}^{M}(x_i^{exp} - x_i^{calc})^2\right]^{1/2} \qquad (35)$$

$$\sigma_y = 100\left[\frac{1}{M}\sum_{i=1}^{M}(y_i^{exp} - y_i^{calc})^2\right]^{1/2} \qquad (36)$$

where σ_P, σ_x, and σ_y were obtained with the optimal values of the binary interaction parameters, and they are given in Table 4. This table shows the correlative capabilities of the PR and PC-SAFT equations by using the van der Waals one-fluid mixing rules and a temperature-independent binary interaction parameter for the $N_2 + C_{10}H_{22}$ system. Overall, it can be said that the quality for correlating the experimental vapor−liquid equilibrium data of this binary system with the PC-SAFT equation is superior to that obtained with the PR equation. The fits of the PR and PC-SAFT equations of state to the $N_2 + C_{10}H_{22}$ system are shown in Figures 5 and 6, respectively.

Figure 5 shows that the PR equation fits the data well at low and moderate pressures, but it is less satisfactory when temperature and/or pressure increase. The fact that predictions at the different temperatures are not precise indicates that a temperature-dependent interaction parameter is necessary to adequately model the $N_2 + C_{10}H_{22}$ system when calculations are made over a wide range of temperatures, as done by Privat et al.[2,3] for the PPR78 model (a group contribution method for estimating binary interaction parameters of the PR equation). Nonetheless, this is outside the scope of this work, and no attempt was made to either determine this temperature dependence or apply other complex mixing rules or combining rules.

Figure 6 shows the results of the correlation with the PC-SAFT equation. In this figure, it can be seen that the overall agreement between experimental and calculated values is quite satisfactory, especially at the highest temperatures. The superior quality of the PC-SAFT equation for predicting the phase behavior of asymmetric mixtures is due to this model being based on a perturbation theory for chain molecules that can be

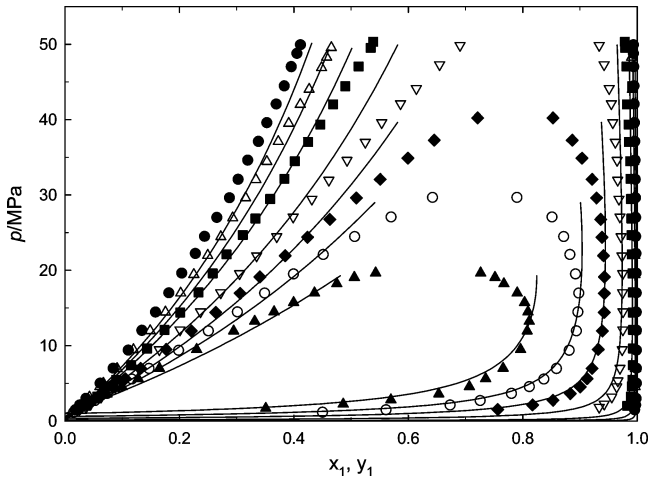

Figure 5. Experimental and calculated pressure−composition phase diagram for the N_2 (1) + $C_{10}H_{22}$ (2) system: ●, 344.6 K; △, 377.4 K; ■, 410.9 K; ▽, 463.7 K; ◆, 503.0 K; ○, 533.5 K; ▲, 563.1 K. Solid lines: PR EoS with $k_{ij} = 0.1597$ fitted to the vapor−liquid equilibrium data of this work.

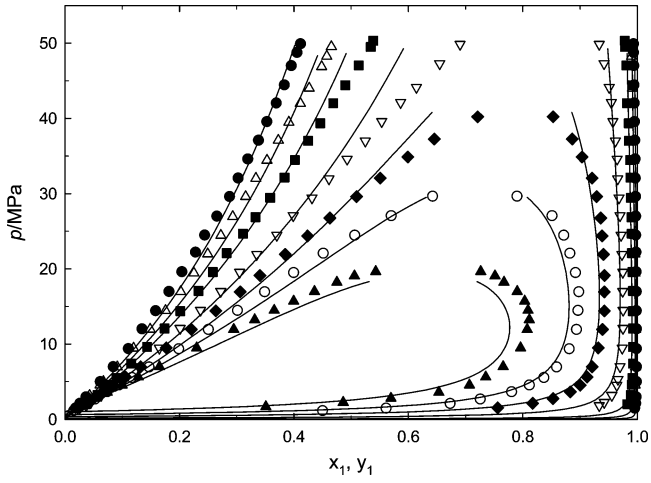

Figure 6. Experimental and calculated pressure−composition phase diagram for the N_2 (1) + $C_{10}H_{22}$ (2) system: ●, 344.6 K; △, 377.4 K; ■, 410.9 K; ▽, 463.7 K; ◆, 503.0 K; ○, 533.5 K; ▲, 563.1 K. Solid lines: PC-SAFT EoS with $k_{ij} = 0.1329$ fitted to the vapor−liquid equilibrium data of this work.

applied to mixtures of small spherical molecules such as gases, nonspherical solvents, and chainlike polymers by using conventional one-fluid mixing rules.

Conclusions

New experimental vapor−liquid data have been obtained for the N_2 + $C_{10}H_{22}$ system at temperatures from (344 to 563) K and at pressures up to 50 MPa by using an experimental static-analytical apparatus with pneumatic capillary samplers. The smoothness of the equilibrium ratio−pressure curve for each isotherm showed suggests a low level of the random errors in the measurements. The phase equilibrium measurements on the system N_2 + $C_{10}H_{22}$ suggest that it belongs to the type III class of systems according to the classification of van Konynenburg and Scott.

The PR and PC-SAFT equations of state with van der Waals one-fluid mixing rules were used to represent the measured data of this binary system by adjusting a single temperature-independent interaction parameter for each equation. Results of the representation showed that the PR equation fit the data well at low and moderate pressures but was less satisfactory at higher temperatures and/or pressures, while thePC-SAFT equation better fit the data over the whole temperature and pressure range studied.

Acknowledgment

The authors thank Professor Gerhard M. Schneider for providing us with a copy of the doctoral dissertation of Michael Wirths.

Literature Cited

(1) García-Sánchez, F.; Eliosa-Jiménez, G.; Silva-Oliver, G.; Vázquez-Román, R. Vapor-Liquid Equilibria of Nitrogen-Hydrocarbon Systems Using the PC-SAFT Equation of State. *Fluid Phase Equilib.* **2004**, *217*, 241–253.

(2) Privat, R.; Jaubert, J. N.; Mutelet, F. Addition of the Nitrogen Group to the PPR78 Model (Predictive 1978 Peng Robinson EOS with Temperature-Dependent k_{ij} Calculated through a Group Contribution Method). *Ind. Eng. Chem. Res.* **2008**, *47*, 2033–2048.

(3) Privat, R.; Jaubert, J. N.; Mutelet, F. Use of the PPR78 Model to Predict New Equilibrium Data of Binary Systems Involving Hydrocarbons and Nitrogen. Comparison with Other GCEOS. *Ind. Eng. Chem. Res.* **2008**, *47*, 7483–7489.

(4) Van Konynenburg, P. H.; Scott, R. L. Critical Lines and Phase Equilibria in Binary Van der Waals Mixtures. *Phil. Trans. R. Soc. London, Ser. A.* **1980**, *298*, 495–540.

(5) De Leeuw, V. V. Phase Behavior of Selected Nitrogen + Hydrocarbon Systems. A Study for Enhanced Oil Recovery in North Sea Fields by Nitrogen Flooding. Doctoral Dissertation, Delft University of Technology, The Netherlands, 1995.

(6) Mungan, N. Enhanced Oil Recovery with High Pressure Nitrogen Injection Paper SPE 62547 presented at the 2000 SPE/AAPG Western Regional Meeting, Long Beach, CA, 19−23 June, **2000.**

(7) Silva-Oliver, G.; Eliosa-Jiménez, G.; García-Sánchez, F.; Avendaño-Gómez, J. R. High-Pressure Vapor-Liquid Equilibria in the Nitrogen-n-Pentane System. *Fluid Phase Equilib.* **2006**, *250*, 37–48.

(8) Eliosa-Jiménez, G.; Silva-Oliver, G.; García-Sánchez, F.; de Ita de la Torre, A. High-Pressure Vapor-Liquid Equilibria in the Nitrogen + n-Hexane System. *J. Chem. Eng. Data* **2007**, *52*, 395–404.

(9) García-Sánchez, F.; Eliosa-Jiménez, G.; Silva-Oliver, G.; Godínez-Silva, A. High-Pressure (Vapor-Liquid) Equilibria in the (Nitrogen + n-Heptane) System. *J. Chem. Thermodyn.* **2007**, *39*, 893–905.

(10) Silva-Oliver, G.; Eliosa-Jiménez, G.; García-Sánchez, F.; Avendaño-Gómez, J. R. High-Pressure Vapor-Liquid Equilibria in the Nitrogen-n-Nonane System. *J. Supercrit. Fluids* **2007**, *42*, 36–47.

(11) Peng, D.-Y.; Robinson, D. B. A New Two Constant Equation of State. *Ind. Eng. Chem. Fundam.* **1976**, *15*, 59–64.

(12) Gross, J.; Sadowski, G. Perturbed-Chain SAFT: An Equation of State Based on Perturbation Theory for Chain Molecules. *Ind. Eng. Chem. Res.* **2001**, *40*, 1244–1260.

(13) Guilbot, P.; Valtz, A.; Legendre, H.; Richon, D. Rapid On-Line Sampler-Injector: a Reliable Tool for HT-HP Sampling and On-Line GC Analysis. *Analusis* **2000**, *28*, 426–431.

(14) Battino, R.; Banzhof, M.; Bogan, M.; Wilhelm, E. Apparatus for Rapid Degassing of Liquids. Part III. *Anal. Chem.* **1971**, *43*, 806–807.

(15) Azarnoosh, A.; McKetta, J. J. Nitrogen-n-Decane System in the Two-Phase Region. *J. Chem. Eng. Data* **1963**, *8*, 494–496.

(16) Llave, F. M.; Chung, T. H. Vapor-Liquid Equilibria of Nitrogen-Hydrocarbon Systems. *J. Chem. Eng. Data* **1988**, *33*, 123–128.

(17) Tong, J.; Robinson, R. L., Jr.; Gasem, K. A. M. Solubilities of Nitrogen in Heavy Normal Paraffins from 323 to 423 K at Pressures to 18.0 MPa. *J. Chem. Eng. Data* **1999**, *44*, 784–787.

(18) Prausnitz, J. M.; Benson, P. R. Solubility of Liquids in Compressed Hydrogen, Nitrogen, and Carbon Dioxide. *AIChE J.* **1959**, *5*, 161–164.

(19) D'Avila, S. G.; Kaul, B. K.; Prausnitz, J. M. Solubilities of Heavy Hydrocarbons in Compressed Methane and Nitrogen. *J. Chem. Eng. Data* **1976**, *21*, 488–491.

(20) Pearce, D. L.; Peters, C. J.; de Swaan Arons, J. Measurements of the Gas Phase Solubility of Decane in Nitrogen. *Fluid Phase Equilib.* **1993**, *89*, 335–343.

(21) Reid, R. C.; Prausnitz, J. M.; Poling, B. E. *The Properties of Gases and Liquids*, 4th ed.; McGraw-Hill: New York, 1987.

(22) Wirths, M. Fluid-Phasengleichgewichte und kritische Erschinungen binärer Mischungen von Kohlenwasserstoffen mit Tetrafluormethan, Trifluormethan und Stickstoff zwischen 273 K und 630 K und bei Drücken bis 250 MPa Doctoral Dissertation, University of Bochum, Germany, 1983.

(23) Christiansen, L. J.; Fredenslund, A. Thermodynamic Consistency Using Orthogonal Collocation or Computation of Equilibrium Vapor Compositions at High Pressures. *AIChE J.* **1975**, *21*, 49–57.

(24) Won, K. W.; Prausnitz, J. M. High-Pressure Vapor-Liquid Equilibria. Calculation of Partial Pressures from Total Pressure Data. Thermodynamic Consistency. *Ind. Eng. Chem. Fundam.* **1973**, *12*, 459–463.
(25) Chen, S. S.; Kreglewski, A. Applications of the Augmented Van der Waals Theory of Fluids. I. Pure Fluids. *Ber. Bunsen-Ges. Phys. Chem.* **1977**, *81*, 1048–1052.
(26) Justo-García, D. N.; García-Sánchez, F.; Romero-Martinez, A. Isothermal Multiphase Flash Calculations with the PC-SAFT Equation of State. *Am. Inst. Phys. Conf. Proc.* **2008**, *979*, 195–214.
(27) Ambrose, D. *Vapour-Liquid Critical Properties*, NPL Report Chemistry 107; National Physical Laboratory: Teddington, 1980.
(28) Nelder, J. A.; Mead, R. A. Simplex Method for Function Minimization. *Comput. J.* **1965**, *7*, 308–313.
(29) Wegstein, J. H. Accelerating Convergence for Iterative Processes. *Comm. Assoc. Comp. Mach.* **1958**, *1*, 9–13.

Received for review November 19, 2008. Accepted February 1, 2009. This work was supported by the Molecular Engineering Research Program of the Mexican Petroleum Institute under Projects D.00406 and I.00432. G. E.-J. gratefully acknowledges the National Council for Science and Technology of Mexico (CONACYT) for the financial support (grant 76894) received through the Program of Repatriation under their Modality of Retention 2007.

JE800881T